ISSN: 1687-1006 p
ISSN: 2682-3640 e

The Egyptian International Journal of Engineering Sciences and Technology

Vol. 36 (2021)33–42

https://eijest.journals.ekb.eg/

Damage Prediction and Evolution Using Uncoupled Elastoplastic-Damage Lemaitre's and Vaz's Models

Mohamed A. El-Shourbagy*, Mohamed A. Attia and Ahmed G. El-Shafei

Department of Mechanical Design and Production Engineering, Faculty of Engineering, Zagazig University P.O. Box 44519, Zagazig, Egypt

ARTICLE INFO

Keywords:

Damage
Lemaitre's damage model
Plasticity
Finite element
Damage variable
Fracture indicator

ABSTRACT

This paper presents the two uncoupled elastoplastic-damage models; uncoupled Lemaitre's and Vaz's damage models. The two models are implemented into the finite element ABAQUS software using user routine UMAT to analyze and predict damage and damage evolution. In the context of von-Mises yield criteria, the damage variable and fracture indicator are predicted, in addition to the von-Mises stress and the effective plastic strain. Both the elastoplastic tangent operator and the return mapping procedure are formulated using the consistent formulation. Two cases are analyzed; the first one is an axisymmetric notched bar, while the second case is a plane strain doubled notched plate. In addition to the aforementioned predictions, a parametric study is carried out to explore the effect of the damage denominator and damage exponent on the damage behavior. It is concluded that the two models succeeded in the prediction of the point of fracture, while the uncoupled Lemaitre's damage model gives a more efficient description of the damage band.

1. Introduction

Elastoplastic analyses have a complicated nature because the stress is normally a function of the history of strain. Due to the complication of equations, closed-form solutions are not valid to the plurality of these problems, and therefore, numerical methods are usually used for solving the problem [1].

The Prandtl–Reuss model which is called J_2-flow theory, is widely used in computational elasto-plasticity. In the classical form of the J_2-flow theory, the materials are characterized by an isotropic strain hardening model or an elastic-perfectly plastic model. In the last five decades, a huge number of contributions were produced to modify the model to include the complexity of the behavior of materials; anisotropy, linearity, and nonlinearity of kinematic hardening, strain rate dependence, softening, and damage [2-5].

At the level of the updating procedure of stress, the integration of the elastoplastic constitutive equations can be performed numerically or by exact integration [6]. The implicit integration scheme is one of the important techniques in which the stress and the plastic variables are updated at the end of the load step. Generally, nonlinear equations in implicit methods should be solved using an iterative process like Newton-Raphson [1].

The work with the implicit integration is initiated by Wilkins [7] who suggested an algorithm for the return mapping of the von-Mises perfect plasticity. Then, Kreig and Key [8] modified the integration by

* Corresponding author. Tel.: +02-01093742508
E-mail address: ma.elshourbagy@gmail.com

adding the effects of the kinematic and isotropic hardening into the model of plasticity. The algorithm for the plane stress case was presented by Simo and Taylor [9]. Also, Ortiz and Popov [10] and Dodds [11] compared several different integration schemes and found that the return mapping technique is better than the other techniques. Later, Hopperstad and Remseth [12] along with Kobayashi and Ohno [13] applied the return mapping algorithm to cyclic plasticity. For more details about numerical integration techniques, see [14-16].

In the damage mechanics area, Kachanov [17] developed the first framework for the damage mechanism which includes the damage due to creep. In the field of damage in elastoplastic analyses, Lemaitre [18] presented his damage model in its uncoupled elastoplastic-damage version and coupled version. Then, Lemaitre [19, 20] and Lemaitre et al. [21, 22] presented their full coupled elastoplastic-damage model which made the base for a lot of works by many researchers. De Souza [15, 23] put an algorithm for fast integration of the constitutive damage equations of the Lemaitre full coupled damage model and called it the simplified Lemaitre model which is considered as an effective model for damage evolution. Vaz and Bressan [24] and Vaz et al. [25, 26] presented their uncoupled criteria for damage evolution and called it the "fracture indicator" which is a useful and effective tool to indicate the damage location.

Generally, the uncoupled damage models are simple. These models assume that the damage state of the structure does not affect the state of strain or stress, i.e., there is decoupling between the constitutive equations of strain and damage. This critical assumption is not bad as far as the calculations of the structure are not too accurate [18]. The uncoupled models are effective fast tools that are suitable for design purposes [27].

In this paper, the damage behavior of ductile materials is predicted and evaluated in the framework of von-Mises yield criteria and uncoupled Lemaitre's and Vaz's damage models. Employing the elasto-plastic consistent formulation, a user subroutine for plasticity and damage evolution is implemented into ABAQUS software. The present model capable of evaluating the damage variables; damage variable and fracture indicator, von-Mises stress, and the effective plastic strain. After mesh sensitivity analysis, a parametric study is conducted to investigate the impact of the damage denominator and damage exponent factors on the deformation and damage behavior of two example problems.

2. Comparison of Models

In any damage model, there is a variable that is used to evaluate the damage state in the domain. In the coming sections, the differences in the damage evolution variables will be represented.

2.1. Uncoupled elastoplastic-damage Lemaitre model.

Assume a cylinder under unidirectional tensile load and the area carrying the load is *A*. During the tensile loading, there are micro-voids appear in the cylinder. Thus, the area that carries the load is reduced to the so-called effective area *A**. The damage variable that evaluates the damage state in the domain is simply equal,

$$\Omega = 1 - \frac{A^*}{A} \tag{1}$$

It is noticed that $\Omega = 0$ corresponds to the undamaged state, while $\Omega = \Omega_c$, where Ω_c, is a material parameter identifying a certain critical value at which crack initiates [18, 28].

To extract an equation for the damage variable in ductile materials, Lemaitre [18] made a mathematical proof based on the assumption that damage in ductile material starts after the material interning to the plastic zone. To achieve that, the equation of the damage variable can be expressed as

$$d\Omega = \left(\frac{-Y}{r}\right)^s d\bar{\varepsilon}^p \tag{2}$$

where $d\bar{\varepsilon}^p$ is the incremental effective plastic strain, and *r* and *s* are respectively, experimentally obtained material parameters, defined as the damage denominator and the damage exponent. The damage energy release rate *Y* is given by [15].

$$Y = \frac{-q^2}{2E(1-\Omega)^2}\left[\frac{2}{3}(1+\nu) + 3(1-2\nu)\left(\frac{p}{q}\right)^2\right] \tag{3}$$

where *p* and *q* are the mean and von-Mises equivalent stresses, respectively, *E* is Young's modulus, and *v* is Poisson's ratio.

2.2. The Uncoupled elastoplastic-damage *Vaz's model.*

Vaz [24] proposed a fracture indicator based on the total damage work. Based on the proposed Vaz criterion, the fracture detector I_D is obtained using the

integration through the whole loading path until the damage variable reaches its critical value Ω_c [24-26],

$$dI_D = (1-\Omega)^{2s} d\Omega = (1-\Omega)^{2s} \left(\frac{-Y}{r}\right)^s d\bar{\varepsilon}^p \qquad (4)$$

3. Constitutive Model

The basic elastoplastic equations used in the present work are based on the work presented in [14, 15] for plane strain and axisymmetric cases.

The law of linear elasticity,

$$\boldsymbol{\sigma} = \boldsymbol{D}^e : \boldsymbol{\varepsilon}^e \qquad (5)$$

where $\boldsymbol{D}^e$ is the isotropic elasticity matrix, $\boldsymbol{\sigma}$ and $\boldsymbol{\varepsilon}^e$ are, respectively, the stress and elastic strain vectors.

The von-Mises yield function can be expressed as

$$\emptyset(\boldsymbol{\sigma}, \sigma_y) = \sqrt{3J_2(\boldsymbol{s}(\boldsymbol{\sigma}))} - \sigma_y \qquad (6)$$

where $\emptyset$ is the yield function, J_2 is the second invariant of the stress deviator $\boldsymbol{s}$, where $J_2 = 0.5\|s\|^2$, and σ_y is the current yield strength, which is a function of effective plastic strain $\bar{\varepsilon}^p$, such that

$$\sigma_y = \sigma_y(\bar{\varepsilon}^p) \qquad (7)$$

The associative flow rule may be written as

$$\Delta\boldsymbol{\varepsilon}^p = \Delta\gamma \frac{\partial \emptyset}{\partial \boldsymbol{\sigma}} = \Delta\gamma\, \boldsymbol{N} \qquad (8)$$

where $\Delta\boldsymbol{\varepsilon}^p$ is the incremental plastic strain vector and $\Delta\gamma$ is the incremental plasticity multiplier. The (Prandtl–Reuss) flow vector $\boldsymbol{N}$ is given by

$$\boldsymbol{N} = \frac{\partial \emptyset}{\partial \boldsymbol{\sigma}} = \sqrt{3/2}\, \frac{\boldsymbol{s}}{\|\boldsymbol{s}\|} \qquad (9)$$

With $\Delta\bar{\varepsilon}^p$ be the incremental effective plastic strain, the associative hardening rule, with the evolution equation for the hardening internal variable is given by

$$\Delta\bar{\varepsilon}^p = \sqrt{2/3}\, \|\Delta\boldsymbol{\varepsilon}^p\| = \Delta\gamma \qquad (10)$$

For small deformation assumption, the total incremental strain vector $\Delta\boldsymbol{\varepsilon}$ can be written as

$$\Delta\boldsymbol{\varepsilon} = \Delta\boldsymbol{\varepsilon}^e + \Delta\boldsymbol{\varepsilon}^p \qquad (11)$$

and the hardening rule and the hardening slope H can be defined as

$$\sigma_y = \begin{cases} \sigma_y^0 + K_p \bar{\varepsilon}^p \\ \sigma_y^0 + R_\infty\left(1 - e^{-\gamma\bar{\varepsilon}^p}\right) \end{cases} \qquad (12)$$

The upper equation in Eq. (12) is the linear hardening rule and the lower is the exponential hardening rule.

$$H = \frac{d\sigma_y}{d\bar{\varepsilon}^p} \qquad (13)$$

where $\Delta\boldsymbol{\varepsilon}^e$ is the incremental elastic strain vector, K_p is the strength coefficient, R_∞ is the hardening infinity variable, and γ is the exponential rule's exponent.

The elastoplastic consistent tangent operator $\boldsymbol{D}^{ep}$ is expressed as [15]

$$\boldsymbol{D}^{ep} = 2G\left(1 - \frac{\Delta\gamma\, 3G}{q}\right)\boldsymbol{I_d} + 6G^2\left[\frac{\Delta\gamma}{q} - \frac{1}{3G+H}\right][\bar{\boldsymbol{N}}_{\boldsymbol{n+1}} \otimes \bar{\boldsymbol{N}}_{\boldsymbol{n+1}}] + K\,\boldsymbol{I} \otimes \boldsymbol{I} \qquad (14)$$

where $\boldsymbol{I}$ denotes the identity matrix, i.e., $\boldsymbol{I} \otimes \boldsymbol{I} = \boldsymbol{I}{:}\,\boldsymbol{I}^{\boldsymbol{T}}$, G is the shear modulus, K is the bulk modulus, and q is the trial effective stress. The deviatoric identity matrix $\boldsymbol{I}_d$ is given by

$$\boldsymbol{I}_d = \begin{bmatrix} 1 & 0 & 0 & 0 \\ 0 & 1 & 0 & 0 \\ 0 & 0 & 0.5 & 0 \\ 0 & 0 & 0 & 1 \end{bmatrix} - \frac{1}{3}\,\boldsymbol{I}{:}\,\boldsymbol{I}^{\boldsymbol{T}} \qquad (15)$$

The elasticity matrix $\boldsymbol{D}^e$,

$$\boldsymbol{D}^{\boldsymbol{e}} = 2G\,\boldsymbol{I_d} + K\,\boldsymbol{I} \otimes \boldsymbol{I} \qquad (16)$$

The triaxiality function f_c,

$$f_c = \sqrt{\frac{2}{3}(1+\nu) + 3(1-2\nu)\left(\frac{p}{q}\right)^2} \qquad (17)$$

Substitution of Eq. (17) into Eq. (3) yields

$$Y = \frac{-q^2}{2E(1-\Omega)^2}\, {f_c}^2 \tag{18}$$

The incremental damage variable $\Delta\Omega$ may be expressed as follows [15, 18, 21, 23, 29, 30]:

$$\Delta\Omega = \left(\frac{-Y}{r}\right)^s \Delta\bar{\varepsilon}^p \tag{19}$$

From Eqs. (4) and (18), the incremental fracture indicator ΔI_D can be written as [24-26]

$$\Delta I_D = \left(\frac{q^2}{2E\, r}\, {f_c}^2\right)^s \Delta\bar{\varepsilon}^p \tag{20}$$

4. Numerical implementation

In the framework of the FEM, the return mapping and updating elastoplastic and damage variables are implemented as follows.

For the $(n+1)^{th}$ load increment;

(I) *Elastic predictor*:

Given $\Delta\boldsymbol{\varepsilon}$ and the state variables, evaluate the elastic trial state using the trial elastic volumetric and deviatoric strains, $\boldsymbol{\varepsilon}_v^{e\,\text{trial}}$ and $\boldsymbol{\varepsilon}_d^{e\,\text{trial}}$, respectively, i.e.

$$\boldsymbol{\varepsilon}^{e\,\text{trial}}_{n+1} = \boldsymbol{\varepsilon}^e_n + \Delta\boldsymbol{\varepsilon}_{n+1}$$
$$\bar{\varepsilon}^{p\,\text{trial}}_{n+1} = \bar{\varepsilon}^p_n$$
$$p^{\text{trial}}_{n+1} = K\varepsilon^{e\,\text{trial}}_{v\,n+1}$$
$$\boldsymbol{s}^{\text{trial}}_{n+1} = 2G\ \boldsymbol{\varepsilon}^{e\,\text{trial}}_{d\,n+1}$$
$$q^{\text{trial}}_{n+1} = \sqrt{{}^3\!/_2\ \boldsymbol{s}^{\text{trial}}_{n+1} : \boldsymbol{s}^{\text{trial}}_{n+1}}$$

(II) *Check plastic admissibility*:

$$q^{\text{trial}}_{n+1} - \sigma_y(\bar{\varepsilon}^{p\,\text{trial}}_{n+1}) \le 0$$

THEN set $(\cdot)_{n+1} = (\cdot)^{\text{trial}}_{n+1}$ and EXIT

ELSE

(III) *Return mapping step*:

Solve the return mapping equation to obtain the plasticity multiplier,

$$\widetilde{\Phi}(\Delta\gamma) = q^{\text{trial}}_{n+1} - 3G\Delta\gamma - \sigma_y\left(\bar{\varepsilon}^p_n + \Delta\gamma\right) = 0$$

(VI) *Update the state variables*:

$$p_{n+1} = p^{\text{trial}}_{n+1}$$

$$\boldsymbol{s}_{n+1} = \left(1 - \frac{3G\Delta\gamma}{q^{\text{trial}}_{n+1}}\right)\boldsymbol{s}^{\text{trial}}_{n+1}$$
$$\boldsymbol{\sigma}_{n+1} = \boldsymbol{s}_{n+1} + p_{n+1}\{1 \quad 1 \quad 0 \quad 1\}^T$$
$$\boldsymbol{\varepsilon}^{\boldsymbol{e}}_{n+1} = \frac{1}{2G}\boldsymbol{s}_{n+1} + \frac{1}{3}\boldsymbol{\varepsilon}^{e\,\text{trial}}_{v\,n+1}\{1 \quad 1 \quad 0 \quad 1\}^T$$
$$\bar{\varepsilon}^p_{n+1} = \bar{\varepsilon}^p_n + \Delta\gamma$$

(V) *Update the damage variables*:

$$f_{c_{n+1}} = \sqrt{{}^2\!/_3\,(1+\nu) + 3(1-2\nu)\left(\frac{p_{n+1}}{q_{n+1}}\right)^2}$$
$$Y_{n+1} = \frac{-q^2_{n+1}}{2E(1-\Omega_n)^2}\, f^2_{C_{n+1}}$$
$$\Delta\Omega_{n+1} = \left(\frac{-Y_{n+1}}{r}\right)^s \Delta\bar{\varepsilon}^p_{n+1}$$
$$\Delta I_{D\,n+1} = \left(\frac{q^2_{n+1}}{2Er} f^2_{C_{n+1}}\right)^s \Delta\bar{\varepsilon}^p_{n+1}$$
$$\Omega_{n+1} = \Omega_n + \Delta\Omega_{n+1}$$
$$I_{D\,n+1} = I_{D\,n} + \Delta I_{D\,n+1}$$

EXIT.

5. Results

In this section, two applications are presented to make the comparison between the uncoupled Lemaitre's and Vaz's damage models. The first one is a notched axisymmetric bar [15], while the second application is a double notched plate [31, 32]. For each application, the von-Mises stress, the effective plastic strain, damage variable, and fracture indicator are predicted. In addition to these outcomes, a parametric study is carried out to find the effect of the damage denominator *r* and the damage exponent *s* on the damage behavior.

5.1. The axisymmetric notched bar

Consider a cylindrical notched bar subjected to axial loading in terms of prescribed displacement U of 0.576 mm, as shown in Fig. 1. Due to symmetry, only one-quarter of the domain is needed to be modeled with eight-node axisymmetric quadrilateral elements, as presented in Fig. 1. The bar material is AISI 1010 (DIN CK10) rolled low carbon steel, with material properties presented in Table 1.

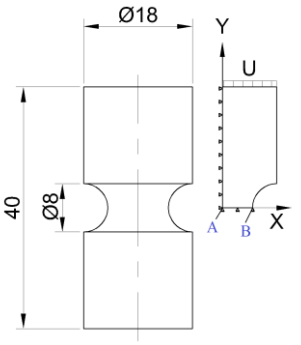

Fig. 1. The geometry of the axisymmetric notched bar.

Table 1. Material mechanical properties [15, 23, 33, 34].

Parameter	Symbol	Value
Modulus of elasticity	E	210 GPa
Poisson's ratio	v	0.3
Yield strength	σ_{y0}	620 MPa
Hardening law	σ_y	$(\sigma_{y0} + 3300[(1 - e^{-0.4\bar{\varepsilon}^p})])$ MPa
Damage denominator	r	3.5 MPa
Damage exponent	s	1.0

Three FE grids are used to study the effect of mesh size on the analysis. Coarse, medium, and fine meshes with 265, 471, and 531 elements, respectively, are used. For the three FE grids, results of the von-Mises stress, effective plastic strain, damage variable, and the fracture indicator at the central point of the bar are presented in Figs. 2-5. It is noticed from Figs. 2 and 3, the values of the von-Mises stress and the effective plastic strain are almost identical in the three cases. The values of the damage variable and the fracture indicator are nearly identical in the case of the medium and fine meshes but lower than their values in the case of coarse mesh, as depicted in Figs. 4 and 5.

Figures 6 and 7 display the distribution of the damage variable and fracture indicator, respectively. In the three FE grids, the maximum damage is found at the central point of the bar, point A shown in Fig. 1. These results are consistent with the prediction of the Lemaitre's coupled elastoplastic-damage model in [15, 23, 33]. Unlike the damage evolution variables, the von-Mises stress and effective plastic strain are found to be maximum at the point B, see Fig. 1.

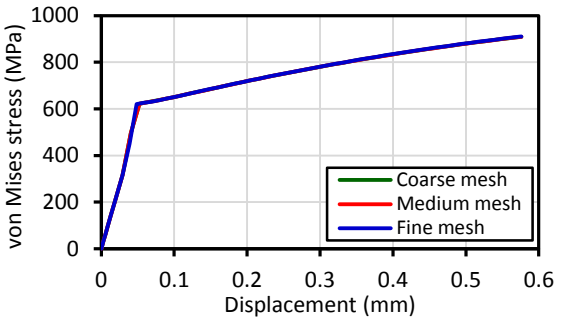

Fig. 2. Variation of von-Mises stress at the central point of the bar with three FE meshes.

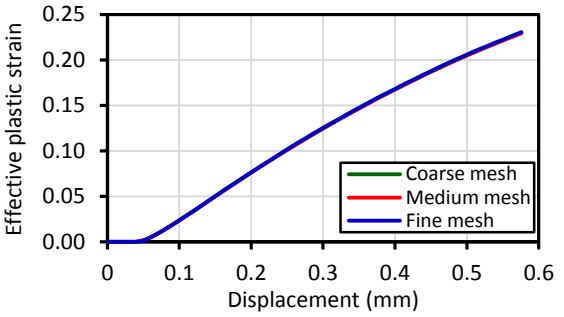

Fig. 3. Variation of effective plastic strain at the central point of the bar with three FE meshes.

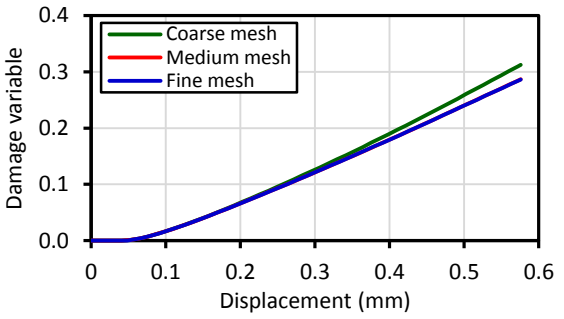

Fig. 4. Variation of the damage variable at the central point of the bar with three FE meshes.

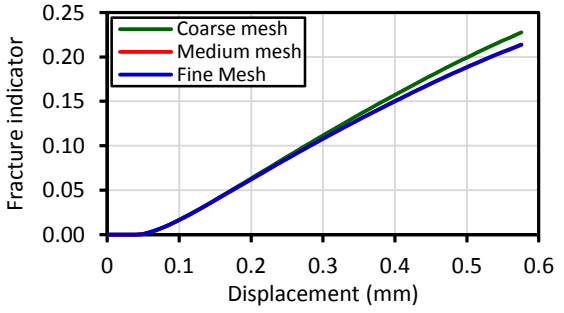

Fig. 5. Variation of the fracture indicator at the central point of the bar with three FE meshes.

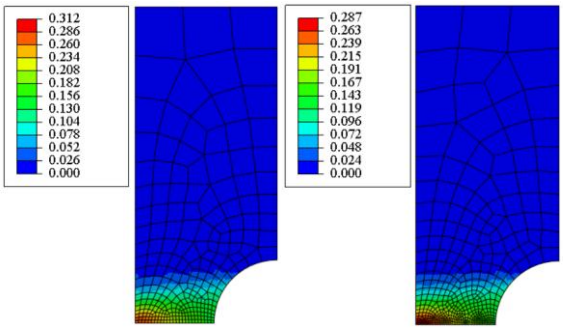

(a) Coarse mesh (b) Medium mesh

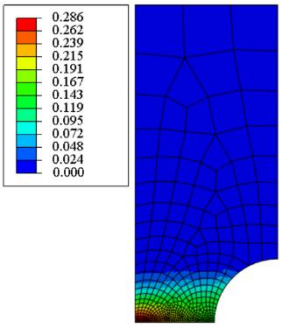

(c) Fine mesh

Fig. 6. The contours of the damage variable for the notched bar for three meshes.

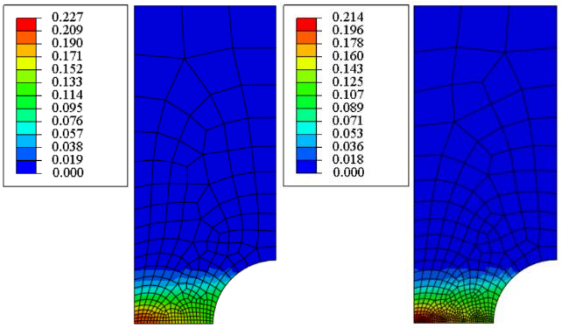

(a) Coarse mesh (b) Medium mesh

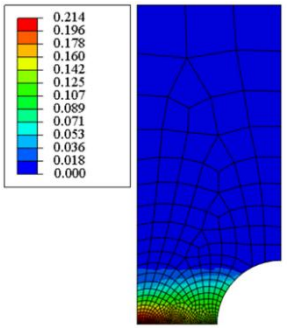

(c) Fine mesh

Fig. 7. The contours of the fracture indicator for the notched bar for three meshes.

A parametric study has been carried out using the medium mesh on the material damage parameters r and s to know their effect on the damage evolution variables. All results are taken at point A, which is the maximum damaged point.

From Figs. 8 and 9, it is noticed that the values of both damage variables and fracture indicator decrease with the increase of parameter r. The reason for these results is that the parameter r is in the denominator of ratio Y/r in Eqs. (2) and (4), respectively, damage variables and fracture indicator.

From Fig. 10, it is noticed that the values of the damage variable increase with the increase of parameter s. On the other hand, the variation of the parameter s has a relatively negligible effect on the fracture indicator, as shown in Fig. 11. Also, the value of the fracture indicator slightly decreases with the increase of the parameter s. This is attributed to that the parameter $(1-\Omega)^{2s}$ is in the nominator in Eq. (4), which defines the fracture indicator. As the value of $0 \leq \Omega \leq 1$, increasing the parameter s decreases the value of $(1-\Omega)^{2s}$, and consequently, the fracture indicator decreases.

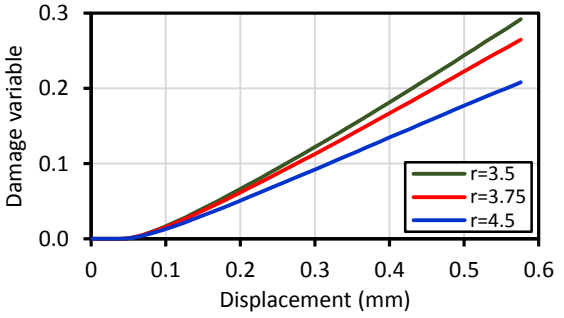

Fig. 8. Variation of the damage variable at the central point of the bar with r parameter.

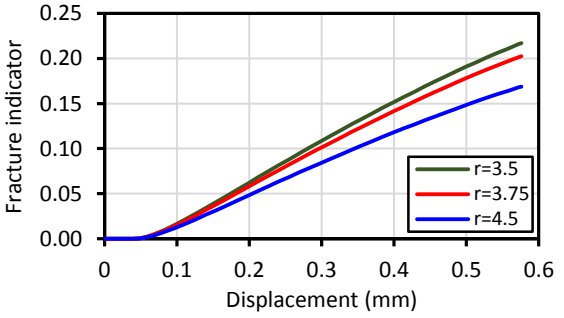

Fig. 9. Variation of the fracture indicator at the central point of the bar with r parameter.

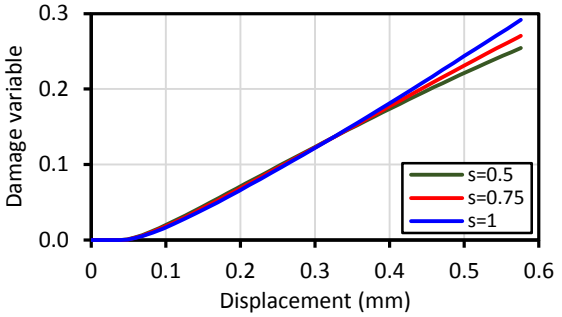

Fig. 10. Variation of the damage variable at the central point of the bar with *s* parameter.

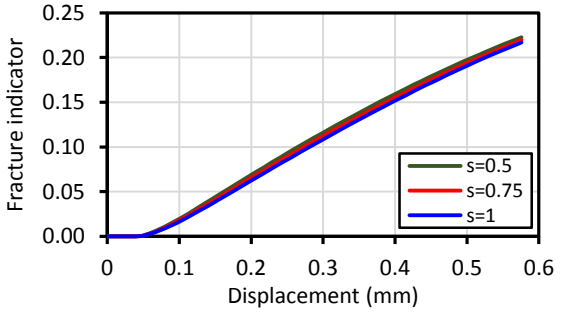

Fig. 11. Variation of the fracture indicator at the central point of the bar with *s* parameter.

5.2. The double notched plate

Consider a double notched plate subjected to axial loading in terms of prescribed displacement U of 0.17 mm, as shown in Fig. 12. Due to symmetry, only one-quarter of the domain is needed to be modeled with eight-node plane strain quadrilateral elements, as presented in Fig. 12. The material properties are presented in Table 2.

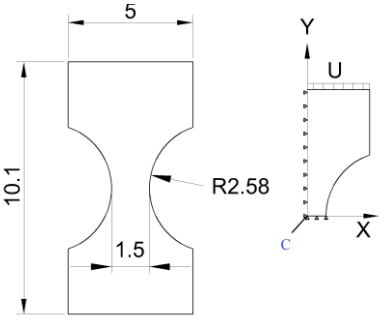

Fig. 12. The geometry of the plain strain double notched plate.

Table 2. Material mechanical properties.

Parameter	Symbol	Value
Modulus of elasticity	E	220 GPa
Poisson's ratio	v	0.3
Yield strength	σ_{y0}	700 MPa
Hardening law	σ_y	$(\sigma_{y0} + 300\bar{\varepsilon}^p)$ MPa
Damage denominator	r	3.0 MPa
Damage exponent	s	1.0

Three FE grids are used to study the effect of mesh size on the analysis. Coarse mesh (42 elements), medium mesh (114 elements), and fine mesh (224 elements). From Figs. 13 and 14, it is noticed that the von-Mises stress and the equivalent plastic strain decrease with the mesh refinement. As the values of the effective plastic strain and von-Mises stress are the main effective variables in the equations of both damage evolution variables, both damage evolution variables decrease with the mesh refinement, as is noticed in Figs. 15 and 16. Also, it is noticed that the damage band in the case of the damage variable is clearer than the fracture indicator's contours. The reason for this non-clarity is the presence of $(1-\Omega)^{2s}$ in the nominator of the incremental fracture indicator's equation (Eq. (4)), which decreases any change in the variables of the equation.

Figures 17 and 18 display the distribution of damage variable and fracture indicator, respectively. In the three FE grids, the maximum damage is found at the central point of the plate (point C), see Fig. 12. These results are consistent with the prediction of the Lemaitre's coupled elastoplastic-damage model in [31, 32]. Like the damage evolution variables, the von-Mises stress and effective plastic strain are found to be maximum at the same point C.

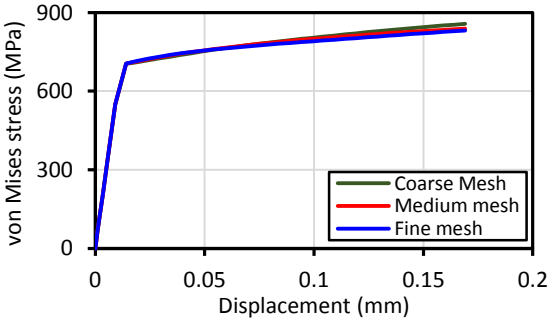

Fig. 13. Variation of von-Mises stress at the central point of the plate with three FE meshes.

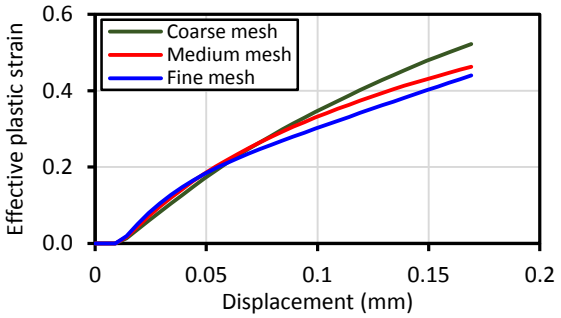

Fig. 14. Variation of effective plastic strain at the central point of the plate with three FE meshes.

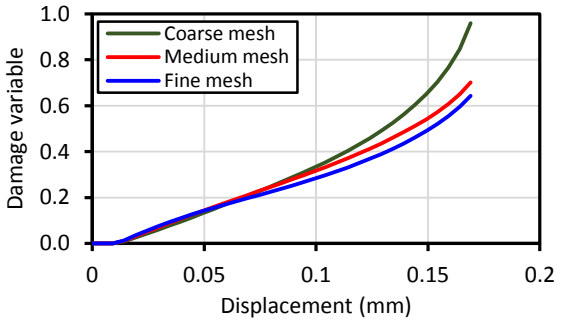

Fig. 15. Variation of the damage variable at the central point of the plate with three FE meshes.

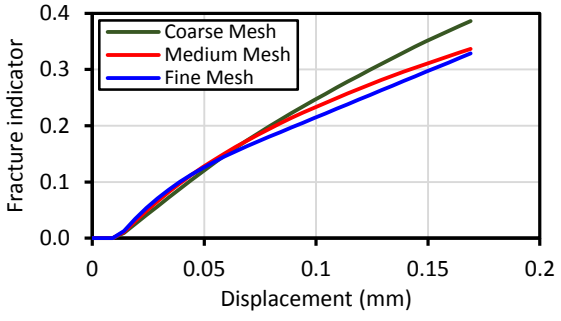

Fig. 16. Variation of the fracture indicator at the central point of the plate with three FE meshes.

The parametric study on the parameters *r* and *s* is carried out on the fine FE mesh. From Figs. 19 and 20, it is noticed that the values of both damage variables and fracture indicator decrease with the increasing of parameter *r*. This is due to that the parameter *r* is in the denominator in Eqs. (2) and (4), respectively, damage variables and fracture indicator.

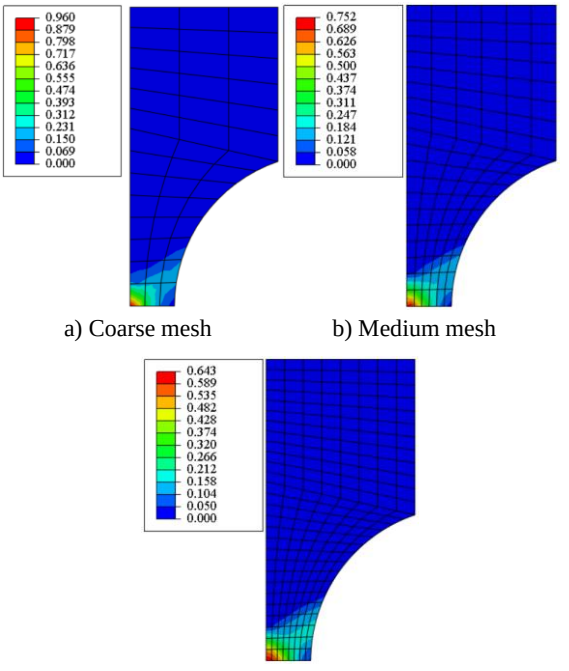

a) Coarse mesh b) Medium mesh

c) Fine mesh

Fig. 17. The contours of the damage variable for the double notched plate for three meshes.

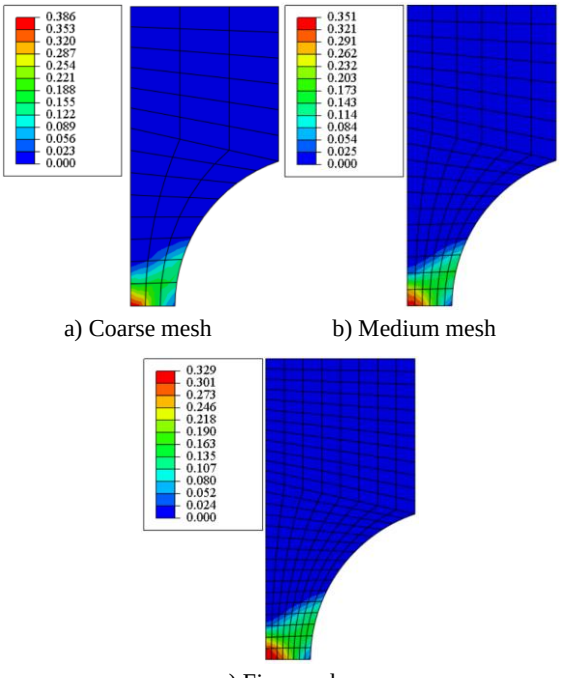

a) Coarse mesh b) Medium mesh

c) Fine mesh

Fig. 18. The contours of the fracture indicator for the double notched plate for three meshes.

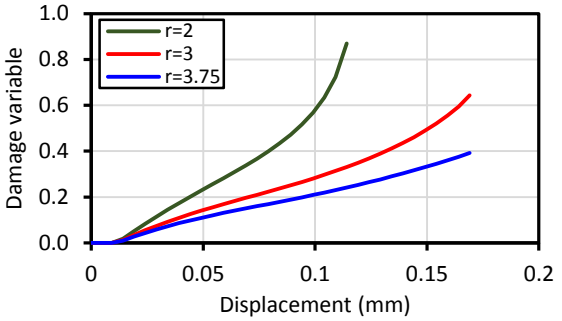

Fig. 19. Variation of the damage variable at the central point of the plate with *r* parameter.

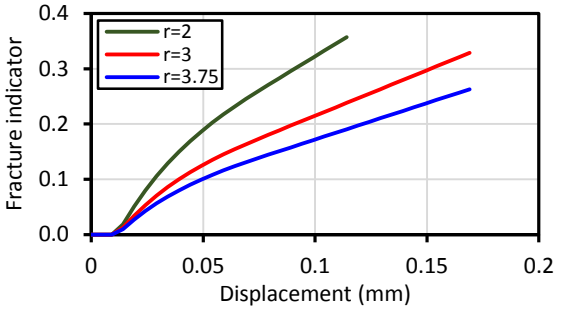

Fig 20. Variation of the fracture indicator at the central point of the plate with *r* parameter.

From Fig. 21 it is noticed that the values of the damage variable increase with the increasing of parameter *s*. On the other hand, from Fig. 22, the values of the fracture indicator decrease with the increase of the parameter *s*. These results are owing to that the term$(1-\Omega)^{2s}$ is in the nominator in Eq. (4) which defined the fracture indicator. As the value of $0 \leq \Omega \leq 1$ which means that the value of $(1-\Omega)^{2s}$ decreases with the increase of the parameter *s* which decreases the value of the fracture indicator.

Comparison of Figs. 8-11 with Figs. 19-22, respectively, shows that the effect of the parameters *r* and *s* on the damage variable and the damage indicator in the double notched plate is greater than that in the notched bar case. This is due to that the predicted effective plastic strain in the double notched plate is much greater than that in the double notched bar, as depicted in Figs. 3 and 14. Also, the geometry of the problem and the material properties significantly contribute to the influence of the parameters *r* and *s* on the damage evolution.

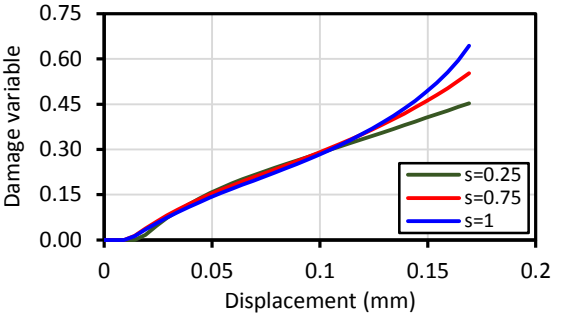

Fig. 21. Variation of the damage variable at the central point of the plate with *s* parameter.

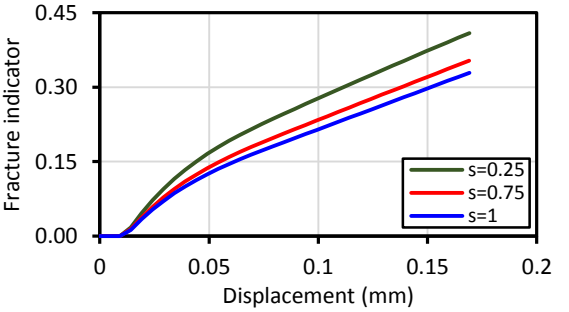

Fig. 22. Variation of the fracture indicator at the central point of the plate with *s* parameter.

6. Conclusion

In the context of von-Mises yield criteria, both uncoupled Lemaitre's and Vaz's damage models are implemented into ABAQUS software using elastoplastic consistent formulation. Damage variable, and fracture indicator, as damage variables, are predicted, in addition to the von-Mises stress and the effective plastic strain. The presented models have succeeded in predicting the point at which fracture initiates. The damage variable is clearer than the fracture indicator in the field of representing the damage band. The uncoupled damage models can be useful in predicting the damage band and the location of the point at which crack initiates. Then after, mesh adaptation is made around that point before running the fully coupled models to minimize the effect of mesh sensitivity. The parametric study that carried out on the effect of damage denominator and damage exponent on the damage behavior showed that the damage variable decreases with increasing damage denominator and increases with the increase of damage exponent. On contrary, the fracture indicator decreases with the increase of both damage denominator and damage exponent.

References

[1] M. Tavoosi, M. Sharifian, and M. Sharifian, "A cross integration for von-Mises plasticity along with nonlinear isotropic hardening and Lemaitre damage model," Iranian Journal of Science and Technology, Transactions of Mechanical Engineering, pp. 1-14, 2020.

[2] R. Hill, The mathematical theory of plasticity. Oxford university press, 1998.

[3] V. A. Lubarda, Elastoplasticity theory. CRC press, 2001.

[4] S. Nemat-Nasser, Plasticity: a treatise on finite deformation of heterogeneous inelastic materials. Cambridge University Press, 2004.

[5] J.-L. Chaboche, "A review of some plasticity and viscoplasticity constitutive theories," International journal of plasticity, vol. 24, no. 10, pp. 1642-1693, 2008.

[6] L. Szabó, "A semi-analytical integration method for J2 flow theory of plasticity with linear isotropic hardening," Computer Methods in Applied Mechanics and Engineering, vol. 198, no. 27-29, pp. 2151-2166, 2009.

[7] M. Wilkins, "Methods in computational physics, volume 3, chapter Calculation of elasticplastic flows," Academic Press, vol. 58, pp. 211-263, 1964.

[8] R. Krieg and S. Key, "Implementation of a time independent plasticity theory into structural computer programs," Constitutive equations in viscoplasticity: Computational and engineering aspects, pp. 125-137, 1976.

[9] J. Simo and R. Taylor, "A return mapping algorithm for plane stress elastoplasticity," International Journal for Numerical Methods in Engineering, vol. 22, no. 3, pp. 649-670, 1986.

[10] M. Ortiz and E. P. Popov, "Accuracy and stability of integration algorithms for elastoplastic constitutive relations," International journal for numerical methods in engineering, vol. 21, no. 9, pp. 1561-1576, 1985.

[11] R. H. Dodds Jr, "Numerical techniques for plasticity computations in finite element analysis," Computers & Structures, vol. 26, no. 5, pp. 767-779, 1987.

[12] O. Hopperstad and S. Remseth, "A return mapping algorithm for a class of cyclic plasticity models," International Journal for Numerical Methods in Engineering, vol. 38, no. 4, pp. 549-564, 1995.

[13] M. Kobayashi and N. Ohno, "Implementation of cyclic plasticity models based on a general form of kinematic hardening," International Journal for Numerical Methods in Engineering, vol. 53, no. 9, pp. 2217-2238, 2002.

[14] J. C. Simo and T. J. Hughes, Computational inelasticity. Springer Science & Business Media, 2006.

[15] E. A. de Souza Neto, D. Peric, and D. R. Owen, Computational Methods for Plasticity: Theory and Applications. John Wiley & Sons, 2011. ISSN: 1119964547, 9781119964544

[16] A. Ochsner, Elasto-plasticity of frame structure elements. Springer, 2016.

[17] L. Kachanov, "On creep rupture time," Izv. Acad. Nauk SSSR, Otd. Techn. Nauk, vol. 8, pp. 26-31, 1958.

[18] J. Lemaitre, "How to use damage mechanics," Nuclear engineering and design, vol. 80, no. 2, pp. 233-245, 1984.

[19] J. Lemaitre, "A continuous damage mechanics model for ductile fracture," 1985.

[20] J. Lemaitre, "Coupled elasto-plasticity and damage constitutive equations," Computer methods in applied mechanics and engineering, vol. 51, no. 1-3, pp. 31-49, 1985.

[21] J. Lemaitre and J.-L. Chaboche, Mechanics of solid materials. Cambridge university press, 1994.

[22] J. Lemaitre, R. Desmorat, and M. Sauzay, "Anisotropic damage law of evolution," European Journal of Mechanics-A/Solids, vol. 19, no. 2, pp. 187-208, 2000.

[23] E. de Souza Neto, "A fast, one- equation integration algorithm for the Lemaitre ductile damage model," Communications in numerical methods in engineering, vol. 18, no. 8, pp. 541-554, 2002.

[24] M. Vaz Jr and J. D. Bressan, "A computational approach to blanking processes," Journal of Materials Processing Technology, vol. 125, pp. 206-212, 2002.

[25] M. Vaz Jr, E. D. S. Neto, and G. Verran, "Numerical and experimental assessment of the ductile fracture process in notched specimens under tensile loading," in CD ROM Proceedings of the VII International Conference on Computational Plasticity, 2003: CIMNE.

[26] M. Vaz Jr and D. Owen, "Numerical simulation of metal cutting using ductile fracture concepts," Computational Mechanics in the UK, pp. 56-59, 1997.

[27] M. Mashayekhi, A. Taghipour, A. Askari, and M. Farzin, "Continuum damage mechanics application in low-cycle thermal fatigue," International Journal of Damage Mechanics, vol. 22, no. 2, pp. 285-300, 2013.

[28] D. Krajcinovic, Damage mechanics. Elsevier, 1996.

[29] J. Lemaitre, "Local approach of fracture," Engineering Fracture Mechanics, vol. 25, no. 5-6, pp. 523-537, 1986.

[30] J. Lemaitre, A course on damage mechanics. Springer Science & Business Media, 2012.

[31] F. Andrade, J. C. de Sá, and F. A. Pires, "Assessment and comparison of non-local integral models for ductile damage," International Journal of Damage Mechanics, vol. 23, no. 2, pp. 261-296, 2014.

[32] E. Azinpour, J. Ferreira, M. P. Parente, and J. C. de Sa, "A simple and unified implementation of phase field and gradient damage models," Advanced Modeling and Simulation in Engineering Sciences, vol. 5, no. 1, pp. 1-24, 2018.

[33] R. L. Gates, "A finite element implementation of a ductile damage model for small strains," arXiv preprint arXiv:1302.2439, 2013.

[34] M. Mashayekhi, S. Ziaei-Rad, J. Parvizian, K. Nikbin, and H. Hadavinia, "Numerical analysis of damage evolution in ductile solids," Structural Durability & Health Monitoring, vol. 1, no. 1, p. 67, 2005.